JACS
JOURNAL OF THE AMERICAN CHEMICAL SOCIETY
Article
pubs.acs.org/JACS

Cell Instructive Microporous Scaffolds through Interface Engineering

Priyalakshmi Viswanathan,[†,‡,#] Somyot Chirasatitsin,[§,#] Kamolchanok Ngamkham,[‡] Adam J. Engler,[*,§,∥,⊥] and Giuseppe Battaglia[*,†,‡]

[†]The Krebs Institute and [‡]Department of Biomedical Science, The University of Sheffield, Sheffield S10 2TN, United Kingdom
[§]Department of Bioengineering and [∥]Material Science Program, University of California, San Diego, La Jolla, California 92093, United States
[⊥]Sanford Consortium for Regenerative Medicine, La Jolla, California 92037, United States

Supporting Information

ABSTRACT: The design of novel biomaterials for regenerative medicine requires incorporation of well-defined physical and chemical properties that mimic the native extracellular matrix (ECM). Here, we report the synthesis and characterization of porous foams prepared by high internal phase emulsion (HIPE) templating using amphiphilic copolymers that act as surfactants during the HIPE process. We combine different copolymers exploiting oil−water interface confined phase separation to engineer the surface topology of foam pores with nanoscopic domains of cell inert and active chemistries mimicking native matrix. We further demonstrate how proteins and hMSCs adhere in a domain specific manner.

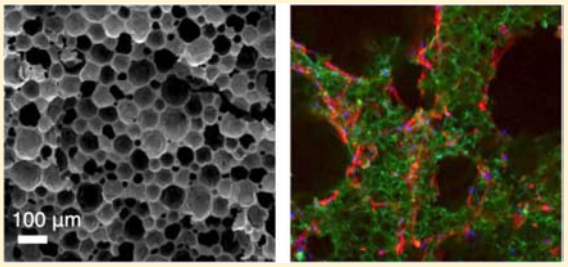

INTRODUCTION

Surface patterning is a key feature of materials science that requires the design of complex structures. Surface topographical features have often been generated through 'top-down' strategies using micro-contact printing or by electron beam-, photo-, or dip pen lithography.[1,2] These techniques provide control over size and arrangement in the micro- and nano-scales with remarkable reproducibility. However, the need for patterned surfaces has extended its niche from the electronics industry to surface chemistry, protein biology, biosensors, and even cell biomechanics.

For biological applications in particular, surface engineering has dominated recent biomaterials design and shown how specific surface functionalities are cell adhesive, for example, carboxyl, amine, or hydroxide groups.[3] The topological arrangement of such chemistries has an equally important effect; the order of nanoscale surface roughness can control and direct cell functions.[2,4] This is particularly critical for stem cell engineering where there is strong requirement to control cell phenotype[4] or direct differentiation.[2] Clustering cell controlling moieties into a more mimetic and well-spaced arrangement can alter cell adhesion and spreading[5] but only when sites are adequately spaced and with sufficient heterogeneity to generate forces.[6] Key biomaterial design aspects must therefore mimic native extracellular matrix (ECM) of the body; they must provide both structural support and intrinsic properties to the cell to influence its behavior,[7] for example, topography,[2] stiffness,[8] and cell binding site spacing[9] and more recently ECM tethering.[10] These cues show exquisite micro- and nanoscopic organization *in vivo*,[9] and in the absence of traditional growth factor cocktails, their spatiotemporal presentation alone can regulate cellular behavior, for example, adhesion, proliferation, differentiation, and apoptosis.[11]

While these efforts highlight how nanoscale topological properties influence cells, most of these studies have been limited to two-dimensional (2D) systems. Three-dimensional (3D) scaffolds often present uniform surface chemistry via surface immobilization or direct cross-linking of a binding motif to the scaffold, yielding either homogeneous or protein polymer hydrogels.[7] Often, however, these materials have very little control over their surface topology, which can be substantially different from native ECM.[9] This suggests the need for rationally designed materials that present cues in a way that reflects ECM's complexity.

Herein we propose the synthesis of a new class of three-dimensional matrices using a 'bottom-up' approach to better mimic the adhesive heterogeneity of matrix and thus control cell adhesion *in vitro*. We propose the combination of high internal phase emulsion (HIPE) templating with interface confined block copolymer self-assembly to engineer 3D porous nanofunctionalized materials as scaffolds for cell culture[12,13] (Figure 1a). To date, the most utilized polyHIPE systems are surfactant-stabilized water-in-oil emulsions, where the oil phase consists of polymerizable monomers, and the controlled combination of polymerization and internal phase destabilization gives rise to highly porous materials.[14] However, such an approach is intrinsically limited by matrix hydrophobicity and the difficulty of introducing surface functionality. One way to introduce hydrophilicity is by preparing 'inverse' oil-in-water

Received: August 28, 2012
Published: November 19, 2012

dx.doi.org/10.1021/ja308523f | J. Am. Chem. Soc. 2012, 134, 20103−20109

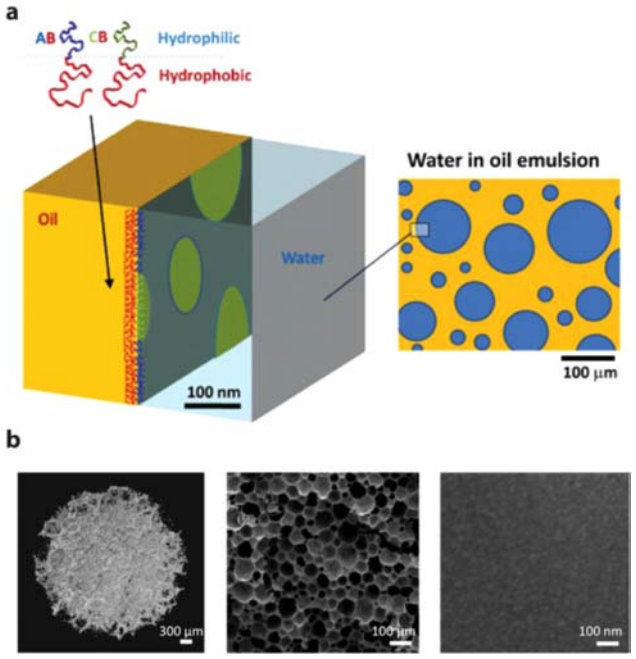

Figure 1. HIPE polymerization scheme. (a) Schematic of high internal phase emulsion templating to form surface cell adhesive and inert domains through amphiphilic block copolymer phase separation at the oil–water interface. (b) Macro- and microporosity of 3D foams shown by X-ray microcomputational tomography (left) and scanning electron micrographs of the foam (center) and the nanoscale surface structure within a pore (right).

polyHIPEs, copolymerizing hydrophilic monomers such as acrylic acid[15] and hydrophilic monomers such as poly(ethylene glycol) methacrylate in water-in-oil emulsions.[16] Surface functionalization of these materials has been achieved with plasma polymerization[17] or polymer grafting through azide–alkyne Huisgen cyclo-addition, which is also known as click chemistry.[18] However, multistep surface modifications often lack control over efficiency. Alternatively, surfactant free Pickering polyHIPEs that utilizes colloidal particles to stabilize the oil–water interface have also been synthesized. For example, PMMA nanoparticles[19] trapped at the oil–water interface upon polymerization may offer control over surface topography in 3D. On the other hand, block copolymers can form nanostructured materials in bulk and in solution by exploiting controlled microphase separation.[20] These nanomaterials have now been translated successfully to control cell adhesion in 2D,[21] but they cannot form structured 3D microenvironments.

Herein we combine the HIPE process with amphiphilic block copolymers polystyrene-*b*-poly(ethylene oxide) (PS-PEO) and/or polystyrene-*b*-poly(acrylic acid) (PS-PAA). What results is a polystyrene (PS)-based foam with high affinity between the amphiphilic copolymer and the PS matrix, anchoring the copolymer at the scaffold surface (Figure 1b). By mixing different amphiphilic copolymers, we can drive the formation of patchy interfaces,[22,23] now with domain size ranging from tens to hundreds of nanometers. Thus, we can design interfaces where cell active motifs (PAA) can be confined on clusters surrounded by inert motifs (PEO) matrix and vice versa (Figure 1a). Furthermore, these foams exhibit architectural features ranging from porosity in the 100 μm range to surface topography in the 10 nm range. We finally demonstrate that stem cells grown on these foams adhere in a block copolymer dependent manner indicating the complexity of adhesive heterogeneity as a cue for stem cell adhesion.

RESULTS

Adhesive Heterogeneity in Extracellular Matrix. Fibronectin, as well as other ECM proteins, have specific cell binding domains, which when assembled into thick matrix fibrils, may be spaced apart from one another or are otherwise inaccessible from cells.[9,24] To first assess how heterogeneous cell accessible adhesion sites are in native matrix, a fibroblast-derived fibronectin matrix was labeled to visualize all matrix fibrils and also regions available for cell adhesion, the latter using 1-μm diameter beads to simulate a cell filopodia that could bind to the matrix. While beads always co-localized with fibrils, their distribution was very heterogeneous throughout the matrix (Supplemental Figure 1a, Supporting Information). Minimum bead-to-bead distance, that is. the length between adhesive sites for cells, was broadly distributed but averaged 3 $\pm$ 1 μm (Supplemental Figure 1b, Supporting Information), reflecting a fairly high degree of adhesive heterogeneity.

PolyHIPE Architecture and Surface Chemistry Modification. HIPEs were produced using combinations of PS-PEO and PS-PAA reported in Table 1. Note that foams will be referred to by their PEO molar content, for example, 25% PEO will be PEO25, except for pure PS-PAA, which will be referred to as PAA100. All foams in this study were 80% porous based on aqueous phase volume using divinylbenzene as the oil phase monomer for all copolymer mixtures. Scanning electron microscopy (SEM) confirmed that all foams contain microscopic porosity regardless of polymer composition (Figure 2a, left). While void distribution is polydisperse, no significant differences in void diameters were observed among mixed formulations. Similarly, higher resolution SEM images showed that foam composition had no qualitative effect on void surface roughness (Figure 2a, right; Supplemental Figure 2a, Supporting Information), allowing any biological response to be compared across the different matrices without bias. For quantitative comparisons of surface morphology, film analogues were synthesized, and when interrogated by atomic force microscopy (AFM), mixtures were found to structurally resemble the foam surface topography regardless of scan size (Figure 2b); maximal height variation was in the submicrometer range for all compositions, though average surface roughness for single copolymer substrates was slightly higher (Supplemental Figure 2b, Supporting Information). The amount of surface roughness previously described to influence cell behavior can be exceedingly small, down to ten(s) of nanometers.[2,25] Thus, we will focus subsequent detection to determine if these scaffolds in combination with its topographical features can determine cell adhesion and spreading in a surface topology dependent manner.

Table 1. Diblock Copolymer Foam Compositions

name	PEO-PS molar fraction	PAA-PS molar fraction
PEO100	100	0
PEO75	75	25
PEO50	50	50
PEO25	25	75
PAA100	0	100

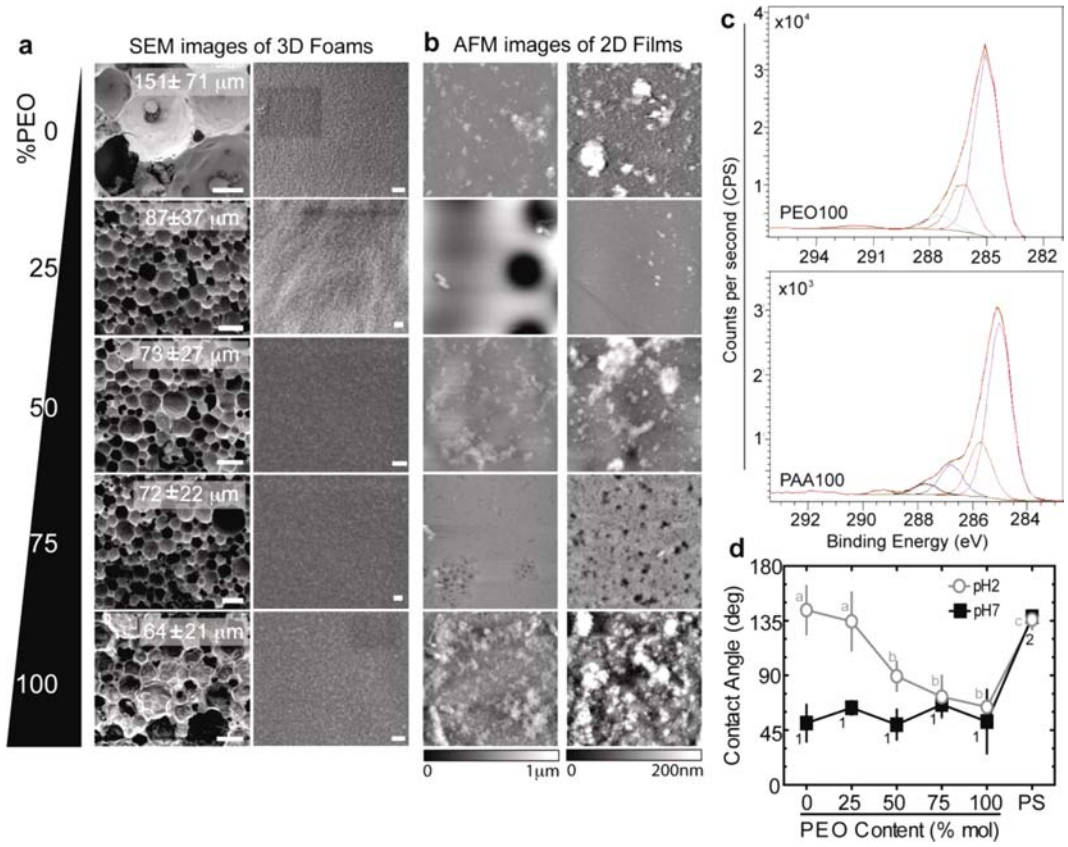

Figure 2. Morphologies of porous foams and films. (a) Scanning electron micrographs of the HIPE foams showing microscale void diameters (mean ± SD; left) and higher magnification images to illustrate surface roughness (right). Scale bars are 100 μm (left) and 100 nm (right). (b) AFM topographs of films from 20 × 20 (left) and 2 × 2 μm scans (right). Image colormap ranges are 0–1 μm and 0–200 nm. (c) X-ray photoelectron spectra of foams containing only polystyrene-*b*-poly(ethylene oxide) or polystyrene-*b*-poly(acrylic acid) copolymers, i.e., PEO100 and PAA100, respectively. (d) Average contact angles of pH 2 (open circles) and pH 7 (closed squares) deionized water on 3D foams as a function of the molar ratio of polystyrene-*b*-poly(ethylene oxide). Mean comparisons of one group versus all samples have the same symbol, e.g., 1, 2, a, b, and c. 1p < 0.05 from pure polystyrene foams. 2p < 0.05 from all other foams at pH 7. ap <0.05 from other mixed composition foams but not polystyrene. p < 0.05 from other copolymer-containing and pure polystyrene foams. p < 0.05 from mixed composition foams PEO50 through PEO100.

As foams appeared more closed porous than traditional polyHIPEs, interconnectivity was assessed by micro computational tomography (Supplemental Figure 2c, Supporting Information). Data representative for PEO 100, PAA100 and its mixture PEO50 confirm interconnectivity of the foams, which is visualized by the 3D rendered image in Figure 1b (left).

While microscopic architecture, that is, porosity and so forth, is important in scaffold design, our aim herein is to successfully functionalize the surface. High-resolution X-ray photoelectron (XPS) C 1s spectra were made for single copolymer foams, that is, PEO100 and PAA100. For PEO100, the C–O signal, detected at 285.0 eV, overlaps with hydrocarbon C–C and C–H bonds, making identification difficult (Figure 2, top). For PAA100 data, however, confirms the COOH group's presence with a distinctive shoulder at 287 eV and a smaller peak appearing at higher energy 289 eV corresponding to the α carbon (C–COOH) and C═O double bonds, respectively (Figure 2c, bottom). To further confirm bulk surface composition, contact angle measurements were employed to investigate composition-dependent changes in macroscopic foam wettability, which can be tuned by pH. At pH 7, contact angles for all block copolymer compositions are significantly lower than the polystyrene/divinylbenzene only foam, for example, SPAN80. Since poly(acrylic acid) has a pK_a of about 4, its side groups make it hydrophilic and hydrophobic in pH above and below its pK_a, respectively. As shown in Figure 2d at pH 2, high PAA-containing foams have a more hydrophobic surface than high PEO-containing foams and are similar in hydrophobicity to polystyrene.

Surface Topology Characterization. Homogenous surface chemistry does not mimic the natural adhesive heterogeneity of matrix[9] and might result in less inductive matrix for cells. As such, we investigated to what extent mixtures of cell adhesive PAA[26] and cell inert PEO[27] block copolymer could undergo interface-confined phase separation in foam morphologies versus the surface domains we have previously observed in amphiphilic polymersomes.[23,28] While bulk metrics identify composition (Figure 2), they cannot identify copolymer phase segregation, and fluorescent detection is complicated by spatial resolution limitations.[23] Chemical force spectroscopy mapping (CFSM)[29] uses a functionalized AFM probe (Supplemental Figure 3a, Supporting Information) to monitor adhesion forces between the probe and film (Supplemental Figure 3b, Supporting Information). Poly-L-lysine (PLL)-functionalized probes mapped adhesive interactions with films of different diblock copolymer composition at 62.5 nm lateral resolution. Though films were maintained at pH 9 to deprotonate PAA and increase its PLL adhesion, PEO100 films appeared to be substantially more adhesive than

dx.doi.org/10.1021/ja308523f | J. Am. Chem. Soc. 2012, 134, 20103–20109

PAA100 (Supplemental Figure 4, Supporting Information), due to counterion screening of the PAA-PLL electrostatic interaction. This may be plausible since negative charges can be screened by free salt typical in quasi-neutral brushes[30] and indicating that PAA chains may have a dense brush configuration.[31] Regardless, differential probe interactions allow us to map the different domains. Using this threshold, CFSM maps and adhesive force histograms were generated for 2 × 2 (Figure 3a, right) and 20 μm × 20 μm scan sizes (Supplemental Figure 5, Supporting Information) for the indicated copolymer compositions to show PEO- (white) and PAA-containing (black) regions. For both scan sizes, PEO area fraction reflected the same increasing trend as in bulk, namely, higher PEO content yields a higher adhesive area fraction (Figure 3c). Domain surface area, defined as a cluster of 4 identical and contiguous observations, were measured from adhesion maps and found to vary from 0.06 to 3.78 μm^2 for PEO (opened squares) and 2.04 to 0.02 μm^2 for PAA (solid circles) as PEO mole fraction increased. ANOVA analysis clearly indicated that low (PAA100 and PEO25) and high (PEO75 and PEO100) PEO mole fraction behaved similarly, reflecting domains of either PEO or PAA, respectively (Figure 3d). The force maps suggest typical bimodal (PEO75, PEO25) and spinodal (PEO50) decomposition patterns as represented by the schematic (Figure 3a, left). In addition to domain surface area, interdomain spacing was also determined between all domains within a given image, for example, Supplemental Figure 6a (Supporting Information) showing PAA domain spacing in PEO75 films. When examining PEO domains, minimum domain-to-domain spacing was greatest when the PEO mole fraction was lowest and nanodomains were present; for PEO fraction >50%, the average spacing was 570 ± 210 nm (Supplemental Figure 6b, Supporting Information). Compared to the bead-to-bead spacing in native matrix of 3 ± 1 μm (Supplemental Figure 1b, Supporting Information), the average minimum domain-to-domain spacing was approximately the same percent standard deviation of 36%. While these two metrics are dissimilar, occur over different length scales, and probed different matrices, the same amount heterogeneity was observed in both measurements. Thus, with increasing PEO composition, domain spacing decreases while size increases (Supplemental Figure 6c, Supporting Information).

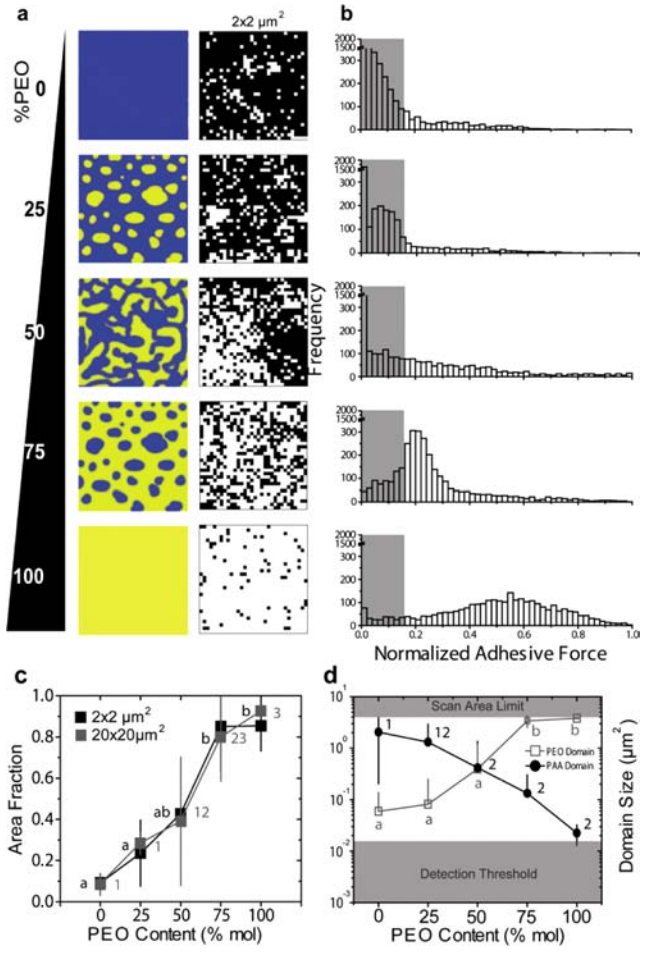

Figure 3. Film characterization by chemical force spectroscopy mapping. (a) Ideal (left) and experimental (right) adhesion images of the distribution of PS-PAA (blue and black regions, respectively) and PS-PEO (yellow and white regions, respectively) shown for a 2 μm × 2 μm scan area with a resolution of 32 × 32 points. (b) Normalized adhesive force distribution as a function of the molar ratio of PS-PEO for all samples. The shaded regions correspond to the threshold for PAA determined in Supplemental Figure 4c) The average PS-PEO area fraction per image was determined as a function of the PS-PEO mole percent for both scan sizes. (d) Average domain surface area of PS-PAA (closed circles) and PS-PEO (open circles). Scan limit indicates the maximum area of the scan and the detection limit is the area of four adjacent measurements. Mean comparisons of one group versus all samples that have the same symbol, e.g., 1, 2, a, and b with $p < 0.05$ versus all data not in the group. By defining adhesion as any value above one standard deviation below the PEO100 film's average adhesion, more than 84% of PEO sites could be identified. Conversely, this threshold correctly identifies nearly all of the PAA100 film's surface (Supplemental Figure 4, shaded box, Supporting Information) and is illustrated again as the gray shaded area in panel b.

Surface mechanics are well-known to play a role in cellular responses[8] especially when coupled with the relatively small pores in the foams which present a 3D environment.[9] The stiffness of copolymer films of varying composition was measured by analyzing the indentation portions of CFSM data. Irrespective of composition, films were nearly rigid, that is, stiffness at or exceeding megapascals (MPa).

Surface Chemistry and Topology Effects on Stem Cells. Having characterized its surface chemistry and topology, how specific surface structures associate with biological function was investigated next. Stem cells in particular are gathering much attention due their ability to differentiate into almost any tissue of our body. Clearly their control and hence the design of cell instructive materials augurs well for regenerative medicine applications. Adhesion and viability was analyzed for human embryonic stem cell derived mesoderm progenitors (hES-MP) (Figure 4a), which are known to differentiate toward adipogenic, myogenic and osteogenic lineages.[32,33] hES-MP viability was measured after a period of 7 days (Figure 4b). It is important to note that hES-MP viability differences were minimal, indicating little if any scaffold toxicity (Supplemental Figure 7, Supporting Information), and thus, cell adhesion differences occurred as a response to the surface chemistry. hES-MP adhesion and spreading were poor on PEO100 foams (Figure 4a), which is not surprising given PEO's nonfouling and biologically inert properties.[27] Interestingly, poor cell adhesion was also seen on 'sticky' PAA100 foams, where the highest cell viability and adhesion would be expected. Instead, cell spreading was highest for hES-MPs on PEO75 and PEO50 foams. High magnification images (Figure 4a) of hES-MPs

dx.doi.org/10.1021/ja308523f | J. Am. Chem. Soc. 2012, 134, 20103−20109

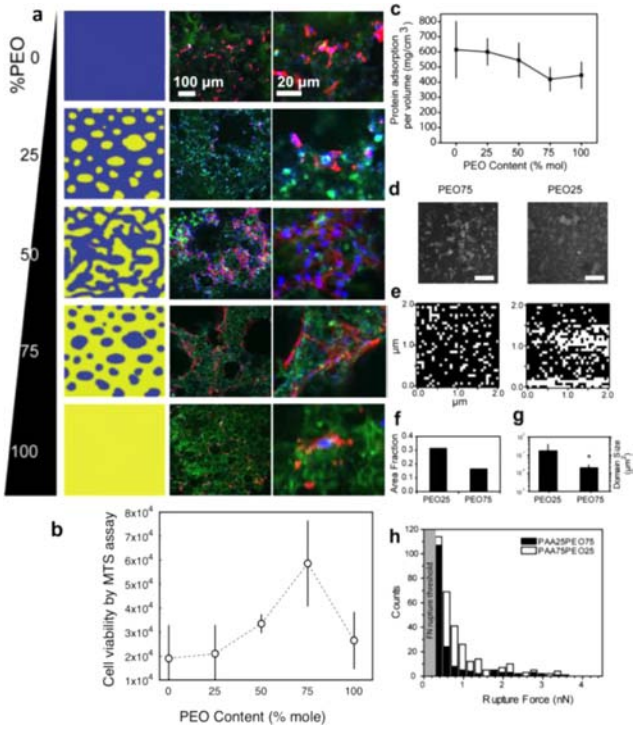

Figure 4. Cell viability and protein adsorption on HIPE scaffolds. (a) Schematic of phase separation of PS-PAA (blue regions) and PS-PEO (yellow regions) are shown as a function of PS-PEO content. Low magnification images of nuclear (blue) and filamentous actin (red) staining of hES-MPs (middle) and high magnification of cell morphology (right) cultured for 7 days on the foams show varying cell attachment and spreading with changing PS-PEO molar ratio. Note that polystyrene within the scaffolds autofluoresces in the green color channel. (b) Average cell number examined by an MTS assay on hES-MPs cultured for 7 days on the 3D foams and plotted versus PS-PEO molar percent. (c) Average total protein adsorption per foam volume. (d) Immunofluorescent staining of fibronectin adsorbed on PEO75 (left) and PEO25 (right) films. Brighter regions represent immobilized fibronectin on the surface. (e) Fibronectin adsorption on PEO75 (left) and PEO25 (right) films detected by CFSM over a 2 μm × 2 μm scan size. White regions represent immobilized fibronectin on the surface. (f) Area fraction of fibronectin adsorption evaluated from CFSM images for foams of indicated PS-PEO content. (g) Average fibronectin domain size determined from CFSM images corresponding to the indicated PS-PEO content. *p < 0.01. (h) Rupture force distribution of the fibronectin−antibody interaction ($F_{threshold}$ = 300 pN; gray shaded region) from fibronectin immobilized on PEO25 (open bar) and PEO75 (closed bar) films.

clearly show highly spread on the PEO75 and PEO50 scaffolds with poor cell adhesion on all other copolymer compositions. Furthermore, SEM micrographs and confocal images (Supplemental Figure 8, Supporting Information) show hES-MPs growing within a 3D matrix. The adhesion pattern of the hES-MPs reflects the total cell number at day 7 (Figure 4b) with the highest number of cells found to be on PEO75 scaffolds. Together, these data would indicate that hES-MPs adhere in a composition-dependent matter, in particular to topologies that mimic the heterogeneity of adhesive sites (PAA domains) in native ECM (Supplemental Figure 1, Supporting Information).

We next sought to ask why cells preferentially adhered to certain surface patterns over others? The answer may rest with which PEO/PAA mixture most closely mimics the natural adhesive heterogeneity of extracellular matrix, providing the appropriate spatial distribution of cell binding and cell inert domains.[9] First, protein adsorption from serum-containing media was measured, but no statistical difference was found in the quantity of serum proteins adsorbed for any foam composition (Figure 4c). While total protein adsorption may not determine how 'adhesive' a specific copolymer composition is to cells, how such proteins might cluster due to specific surface chemistry may correlate with cell adhesion and ultimately behavior. In fact, detection of fibronectin binding to films of PEO75 and PEO25 from serum containing media was examined by confocal microscopy (Figure 4d) and CFSM (Figure 4e), and fibronectin clustering was found to be surface chemistry-dependent (white regions, Figure 4e). The changes in fibronectin's distribution on the surface (Figure 4f) were found to correspond with area fraction changes previously seen with PAA, where protein adsorption should occur due to its opposing charge. Fibronectin bound to PEO75 substrates aggregated into 0.13 μm^2 domains spaced at least 0.52 μm apart (Figure 4g), reflecting the smaller adhesive domains of PAA on PEO75 substrate's surface. On the other hand, larger adhesive domains spaced much closer together in PEO25 approached the scan size limit (Figure 4e) and equated to 50% more rupture events on PEO25 than PEO75 (Figure 4h), together implying a more uniform protein coating. Thus, it would appear that preferential cell adhesion is likely due to protein surface clustering. Together, these data generate 3D matrices using a strategy that exploits macromolecular self-assembly and creates chemically and topologically defined surfaces.

■ DISCUSSION

These data illustrate how scaffold patterns can control protein adsorption and thus cell adhesion in a way that better reflects natural heterogeneity in matrix properties. Other systems, which employ surfaces with discrete, regularly spaced adhesive ligands in 2D,[21,34] have shown differential cell adhesion, spreading, and migration. Cell adhesion and integrin clustering can be reduced or increased by pattern order or disorder, respectively, when interligand spacing exceeds 70 nm.[35] A similar level of disorder is reflected in the adhesive heterogeneity of native matrix observed here and shown elsewhere,[9] and our diblock copolymer foams reflect a similar level of heterogeneity in 3D. We show that our ability to tune the heterogeneity in foams can directly affect protein and subsequent stem cell adhesion in a block copolymer domain dependent manner. Protein adsorption at the cell−matrix interface plays an important role in cell adhesion, particularly on synthetic matrices in the absence of recognizable ligand binding sites. Here, we show that upon 2 h of fibronectin immobilization on the scaffolds, adsorption occurs through the carboxyl groups of the PAA chains with PEO serving as the nonfouling component of the matrix. Studies have shown influence of cell−matrix interactions of surface chemistry on the conformation and assembly of proteins at the interface.[36,37] Hydrophobic surfaces often induce suboptimal conformations of adsorbed serum proteins in that hydrophobic groups are often placed toward the substrate surface. On the other hand, hydrophilic surfaces have been shown to promote adsorption of proteins closer to their native conformations.[38] Resulting changes in protein conformation can therefore alter integrin binding[39] and subsequent cell adhesion. Taken together, our results combine surface chemistry through nonfouling and adhesive groups as well as their topology, implying that an optimal balance between protein concentration and spatial

distribution may be contributing toward the preferential adhesive behavior of the stem cells observed here.

HIPE Template as a Scaffold Template. A HIPE template provides highly tunable physical and chemical characteristics suitable for cell growth and proliferation, for example, pore size, surface roughness, surface chemistry, and so forth. Scaffold pore size typically ranges from 100 to 600 μm to maintain adequate cell infiltration;[40,41] natural biomaterials such as collagen gels sustain excellent cell adhesion and proliferation despite pore sizes of less than 100 μm.[42] Depending on emulsion parameters, HIPE scaffolds here provided pore sizes between 40 and 120 μm while maintaining sufficient adhesion and infiltration. With porosity much closer to natural matrices, this suggests that, as was observed in 2D,[34,43] adhesive domains may in fact encourage migration into the scaffold despite lower pore interconnectivity as larger ligand spacing encourages more labile adhesions.[44] Despite low foam interconnectivity, our data show sufficient cell penetration within a 3D environment during the 7 day culture period. As literature is sparse for block copolymer stabilized HIPEs, understanding its role in emulsion kinetics and as well as the mechanism underlying open and closed porosity with such foams warrants further investigations. These studies will help to further understand the implications of topologically controlled hMSC behavior in long-term cultures.

Most scaffolds with homogeneous surface chemistry do not recapitulate the heterogeneous adhesivity of natural matrix.[9] More recently, spatially controlled surface chemistries have been used to better understand how adhesion formation and even differentiation are affected by heterogeneously distributed adhesions in 2D. RGD peptides spaced at small intervals (<50 nm) favor mature adhesions,[34] spread cells,[21] and osteogenesis,[45] whereas larger intervals (>50 nm) appear to favor an adipogenic fate[46] resulting from dynamic adhesions in less spread cells.[34,44] Given that the link between cell spreading, shape, and fate is due to differences in membrane tension,[47,48] differentiation control by heterogeneous adhesion sites in 2D would appear to have mechanical origins. Scaffold adhesive spots detected by CFSM here were 10-fold larger than the largest domains previously used in these patterned substrates,[29,34,35,44] and thus, they may support fundamentally different types of adhesions. Thus, differences in hES-MP adhesion observed here with HIPE scaffolds containing well-spaced PS-PAA domains versus conventional substrates are most likely the result of adhesive domains reflecting a length scale more representative of heterogeneously adhesive matrix,[9,11] that is, the deviation in adhesion spacing in native fibronectin matrix is similar to that in the foams used here. Thus, how this adhesive behavior reflects on eventual hMSC differentiation and lineage commitment depending on the block copolymer domains remains to be investigated.

■ CONCLUSION

Together, these data show a simple and cost-effective method to generate three-dimensional matrices using a strategy that exploits macromolecular self-assembly. This process results in chemically and topologically defined surfaces that control cell adhesion. The work described here illustrates how topological patterns in a scaffold can control protein adsorption and thus cell adhesion in a way that better reflects the natural differences in matrix properties. While the work describes adsorbed proteins based on inert (PEO) and adhesive (PAA) copolymers, the results suggest that chemistries with tailored presentation of specific cell recognition peptides, for example, RGD, could more directly regulate cell−matrix interactions and mimic matrix even better than these PEO/PAA foams. This work also uses a rigid polystyrene backbone, but as shown with hydrogels, controlling mechanical properties is critically important;[8] changing the oil phase monomers to viscoelastic ethylhexyl acrylate or methacrylate[49] or to biodegradable polycaprolactone[50] and poly(lactic acid),[51] all of which have been previously used in the HIPE process, could further soften these foams and make them more clinically translatable. Finally, the stem cell investigations occurred over one week and were sufficient for cell adhesion, but current HIPE scaffolds may lack sufficient interconnectivity to support cell growth over longer time periods relevant for tissue engineering and regenerative medicine. Regardless of potential modifications, these data show that, with careful choice of block copolymer mixtures, HIPE scaffolds can provide a three-dimensional matrix that presents a cue, adhesive heterogeneity, which has the potential to direct cell behavior.

Abbreviations. hMSC, human mesenchymal stem cell; HIPE, high internal phase emulsion; ECM, extracellular matrix; PS-PEO, polystyrene-*b*-poly(ethylene oxide); PS-PAA, polystyrene-*b*-poly(acrylic acid); PEO25PAA75, polystyrene-*b*-poly(ethylene oxide) 25% mol and/or polystyrene-*b*-poly(acrylic acid) 75% mol; SEM, scanning electron microscopy; AFM, atomic force microscopy; XPS, X-ray photoelectron spectroscopy; PLL, poly-L-lysine; CFSM, chemical force spectroscopy mapping; hES-MP, human embryonic stem cell derived mesoderm progenitors; hBMSC primary human bone marrow derived mesenchymal cells; 2D , two dimensional; 3D, three dimensional.

■ ASSOCIATED CONTENT

Ⓢ Supporting Information

Additional scaffold and 2D film methods and characterization as well as all cell culture information. This material is available free of charge via the Internet at http://pubs.acs.org.

■ AUTHOR INFORMATION

Corresponding Author

aengler@ucsd.edu; g.battaglia@sheffield.ac.uk

Author Contributions

#These authors contributed equally.

Notes

The authors declare no competing financial interest.

■ ACKNOWLEDGMENTS

The authors thank Dr. Gwendolen Reilly (University of Sheffield) for fruitful discussions, Dr. Nicholas Geisse (Asylum Research; Santa Barbara, CA) for technical support and Dr. Adrian Boatwright (University of Nottingham) for XPS assistance. This work was supported by grants from the National Institutes of Health (1DP02OD006460 to A.J.E.), Human Frontiers Science Program (RGY0064/2010 to A.J.E. and G.B.), and the Engineering and Physical Sciences Research Council (EP/F019750/1). Pre-doctoral fellowship support was also provided by the Royal Thai Government Science and Technology (to S.C.).

■ REFERENCES

(1) Ruiz, S. A.; Chen, C. S. *Soft Matter* **2007**, *3*, 1−11.

(2) Dalby, M. J.; Gadegaard, N.; Tare, R.; Andar, A.; Riehle, M. O.; Herzyk, P.; Wilkinson, C. D.; Oreffo, R. O. *Nat. Mater.* **2007**, *6*, 997–1003.
(3) Curran, J. M.; Chen, R.; Hunt, J. A. *Biomaterials* **2006**, *27*, 4783–4793.
(4) McMurray, R. J.; Gadegaard, N.; Tsimbouri, P. M.; Burgess, K. V.; McNamara, L. E.; Tare, R.; Murawski, K.; Kingham, E.; Oreffo, R. O.; Dalby, M. J. *Nat. Mater.* **2011**, *10*, 637–644.
(5) Arnold, M.; Cavalcanti-Adam, E. A.; Glass, R.; Blummel, J.; Eck, W.; Kantlehner, M.; Kessler, H.; Spatz, J. P. *ChemPhysChem* **2004**, *5*, 383–388.
(6) Galbraith, C. G.; Yamada, K. M.; Sheetz, M. P. *J. Cell Biol.* **2002**, *159*, 695–705.
(7) Lutolf, M. P.; Hubbell, J. A. *Nat. Biotechnol.* **2005**, *23*, 47–55. Cukierman, E.; Pankov, R.; Stevens, D. R.; Yamada, K. M. *Science* **2001**, *294*, 1708–1712.
(8) Engler, A. J.; Sen, S.; Sweeney, H. L.; Discher, D. E. *Cell* **2006**, *126*, 677–689.
(9) Reilly, G. C.; Engler, A. J. *J. Biomech.* **2010**, *43*, 55–62.
(10) Trappmann, B.; Gautrot, J. E.; Connelly, J. T.; Strange, D. G. T.; Li, Y.; Oyen, M. L.; Stuart, M. A.; Boehm, H.; Li, B.; Vogel, V.; Spatz, J. P.; Watt, F. M.; Huck, W. T. S. *Nat. Mater.* **2012**, *11*, 642–649.
(11) Hay, E. D. *Cell Biology of Extracellular Matrix*, 2nd ed.; Plenum Press: New York, 1991.
(12) Bokhari, M.; Carnachan, R. J.; Cameron, N. R.; Przyborski, S. A. *Biochem. Biophys. Res. Commun.* **2007**, *354*, 1095–1100.
(13) Bokhari, M.; Carnachan, R. J.; Przyborski, S. A.; Cameron, N. R. *J. Mater. Chem.* **2007**, *17*, 4088–4094.
(14) Carnachan, R.; Bokhari, M.; Przyborski, S. A.; Cameron, N. R. *Soft Matter* **2006**, *2*, 608–616.
(15) Krajnc, P.; Stefanec, D.; Pulko, I. *Macromol. Rapid Commun.* **2005**, *26*, 1289–1293.
(16) Kimmins, S. D.; Wyman, P.; Cameron, N. R. *React. Funct. Polym.* **2012**, *72*, 947–954.
(17) Canal, C.; Gaboriau, F.; Esquena, J. *Plasma Processes Polym.* **2009**, *6*, 686–692.
(18) Cummins, D.; Duxbury, C. J.; Heise, A. *Soft Matter* **2009**, *5*, 804–811.
(19) Gurevitch, I.; Silverstein, M. *Macromolecules* **2012**, *45*, 6450–6456.
(20) Smart, T.; Lomas, H.; Massignani, M.; Flores-Merino, M. V.; Perez, L. R.; Battaglia, G. *Nano Today* **2008**, *3*, 38–46.
(21) George, P. A.; Quinn, K.; Cooper-White, J. J. *Biomaterials* **2010**, *31*, 641–647.
(22) Battaglia, G.; LoPresti, C.; Massignani, M.; Warren, N. J.; Madsen, J.; Forster, S.; Vasilev, C.; Hobbs, J. K.; Armes, S. P.; Chirasatitsin, S.; Engler, A. J. *Small* **2011**, *7*, 2010–2015.
(23) LoPresti, C.; Massignani, M.; Fernyhough, C.; Blanazs, A.; Ryan, A. J.; Madsen, J.; Warren, N. J.; Armes, S. P.; Lewis, A. L.; Chirasatitsin, S.; Engler, A. J.; Battaglia, G. *ACS Nano* **2011**, *5*, 1775–1784.
(24) Mao, Y.; Schwarzbauer, J. E. *Matrix Biol.* **2005**, *24*, 389–399.
(25) Oh, S.; Brammer, K. S.; Li, Y. S.; Teng, D.; Engler, A. J.; Chien, S.; Jin, S. *Proc. Natl. Acad. Sci. U.S.A.* **2009**, *106*, 2130–2135.
(26) Lee, K. Y. *Chem. Rev.* **2001**, *101*, 1869–1880.
(27) Liu, S. Q.; Tay, R.; Khan, M.; Ee, P. L. R.; Hedrick, J. L.; Yang, Y. Y. *Soft Matter* **2009**, *6*, 67–81.
(28) Massignani, M.; LoPresti, C.; Blanazs, A.; Madsen, J.; Armes, S. P.; Lewis, A. L.; Battaglia, G. *Small* **2009**, *5*, 2424–2432.
(29) Chirasatitsin, S.; Engler, A. J. *J.Phys.: Condens. Matter* **2010**, *22*, 194102.
(30) Israels, R.; Leermakers, F. A. M.; Fleer, G. J. *Macromolecules* **1994**, *27*, 3087–3093.
(31) Ballauf, M.; Borisov, O. *Curr. Opin. Colloid Interface Sci.* **2006**, *11*, 316–323.
(32) Peppo, G. M. D.; Svensson, S.; Lenneras, M.; Synnergren, J.; Stenberg, J.; Strehl, R.; Hyllner, J.; Thomsen, P.; Karlsson, C. *Tissue Eng., Part A* **2005**, *16*, 2161–2182.
(33) Pittenger, M. F.; Mackay, A. M.; Beck, S. C.; Jaiswal, R. K.; Douglas, R.; Mosca, J. D.; Moorman, M. A.; Simonetti, D. W.; Craig, S.; Marshak, D. R. *Science* **1999**, *284*, 143–147.
(34) Cavalcanti-Adam, E. A.; Volberg, T.; Micoulet, A.; Kessler, H.; Geiger, B.; Spatz, J. P. *Biophys. J.* **2007**, *92*, 2964–2974.
(35) Huang, J.; Grater, S. V.; Corbellini, F.; Rinck, S.; Bock, E.; Kemkemer, R.; Kessler, H.; Ding, J.; Spatz, J. P. *Nano Lett.* **2009**, *9*, 1111–1116.
(36) Keslowsky, B.; Collard, D.; Garcia, A. *J. Biomed. Mater. Res., Part A* **2003**, *66*, 247–259.
(37) Ayala, R.; Zhang, C.; Yang, D.; Hwang, Y.; Aung, A.; Shroff, S. S.; Arce, F. T.; Lal, R.; Arya, G.; Varghese, S. *Biomaterials* **2011**, *32*, 3700–3711.
(38) Vogler, E. A. *Adv. Colloid Inter. Sci.* **1998**, *74*, 69–117.
(39) Keselowsky, B.; Collard, D. M.; Garcia, A. *Proc. Natl. Acad. Sci. U.S.A.* **2005**, *102*, 5953–5957.
(40) Hollister, S. J. *Nat. Mater.* **2005**, *4*, 518–524.
(41) Karageorgiou, V.; Kaplan, D. *Biomaterials* **2005**, *26*, 5474–5491.
(42) Nehrer, S.; Breinan, H. A.; Ramappa, A.; Young, G.; Shortkroff, S.; Louie, L. K.; Sledge, C. B.; Yannas, I. V.; Spector, M. *Biomaterials* **1997**, *18*, 769–776.
(43) George, P. A.; Donose, B. C.; Cooper-White, J. J. *Biomaterials* **2009**, *30*, 2449–2456.
(44) Selhuber-Unkel, C.; Erdmann, T.; Lopez-Garcia, M.; Kessler, H.; Schwarz, U. S.; Spatz, J. P. *Biophys. J.* **2010**, *98*, 543–551.
(45) Dalby, M. J.; Yarwood, S. J.; Riehle, M. O.; Johnstone, H. J. H.; Affrossman, S.; Curtis, A. S. G. *Exp. Cell Res.* **2002**, *276*, 1–9.
(46) McBeath, R.; Pirone, D. M.; Nelson, C. M.; Bhadriraju, K.; Chen, C. S. *Dev. Cell* **2004**, *6*, 483–495.
(47) Kilian, K. A.; Bugarija, B.; Lahn, B. T.; Mrksich, M. *Proc. Natl. Acad. Sci. U.S.A.* **2010**, *107*, 4872–4877.
(48) Deeg, J. A.; Louban, I.; Aydin, D.; Selhuber-Unkel, C.; Kessler, H.; Spatz, J. P. *Nano Lett.* **2011**, *11*, 1469–1476.
(49) Cameron, N. C.; Sherringdon, D. C. *J. Mater. Chem* **1997**, *7*, 2209–2212.
(50) Lumelsky, Y.; Silverstein, M. S. *Macromolecules* **2009**, *42*, 1627–1633.
(51) Busby, W.; Cameron, N. R.; Jahoda, C. A. B. *Polym. Int.* **2002**, *51*, 871–888.